Estimated States for the CyberShip II Using the Unscented Kalman Filter: A Comparative Simulation

Sajjad Fakhar Shahreza
Dept. Ingeniería
Universidad Loyola Andalucia
Seville, Spain
sfakhar@uloyola.es

Luis Orihuela
Dept. Ingeniería Electrónica, Sistemas Informáticos y Automática
Centro de Investigación en Tecnología, Energía y Sostenibilidad (CITES)
Universidad de Huelva
Huelva, Spain
luis.orihuela@diesia.uhu.es

Guillermo Bejarano
Dept. Ingeniería; Instituto LETS
Universidad Loyola Andalucia
Seville, Spain
gbejarano@uloyola.es

Pablo Millán
Dept. Ingeniería; Instituto LETS
Universidad Loyola Andalucia
Seville, Spain
pmillan@uloyola.es

***Abstract*—This paper presents a model-based Unscented Kalman Filter (UKF) for state estimation of the CyberShip II autonomous surface vessel and compares two nonlinear estimators. The first one, called Filter-IA, is a 12-state Inertial-Aided (IA) filter that includes accelerometer biases, gyroscope bias, and residual acceleration-level disturbances. The second one, named Filter-GN, is a reduced 10-state GNSS Navigation (GN) filter that excludes accelerometer biases. The process model combines Earth-fixed kinematics with an acceleration-level representation of the ship dynamics. The model includes quasi-quadratic hydrodynamic terms and slowly varying residual disturbances. The measurement model of Filter-IA fuses position, heading, body-frame accelerations, and yaw measurements, whereas Filter-GN uses only position, heading, and gyroscope-based yaw measurements. The UKF is implemented in discrete time with a multi-rate structure and is adapted to account for the periodicity of the heading angle. The work focuses on the mathematical formulation of both filters and on their comparative evaluation through simulation.**

***Index Terms*—Autonomous surface vehicles, unscented Kalman filtering, nonlinear observers, sensor fusion.**

I. Introduction

Accurate state estimation is essential for guidance, navigation, and control of vessels, especially when body-fixed velocities are not directly measured [1]. In a typical marine sensor configuration, position is provided by a Global Navigation Satellite System (GNSS), heading is given by an Attitude and Heading Reference System (AHRS) or an electronic compass, and inertial data are measured by an Inertial Measurement Unit (IMU). However, these measurements are affected by noise, bias, and different sampling rates. Thus, a model-based estimator is required to reconstruct the full motion state. This problem becomes more difficult in outdoor and dynamic environments. GNSS performance can be reduced by signal blockage, multipath effects, and intermittent availability [2]. In contrast, IMU-based navigation provides high-rate, continuous measurements but suffers from drift and bias accumulation over time [3]. Therefore, GNSS and IMU measurements are naturally complementary. GNSS provides absolute navigation information, while the IMU preserves short-term motion continuity between GNSS updates [3], [4]. An electronic compass additionally provides heading information, consistent with the use of magnetometer data in GNSS observers to support attitude estimation and gyro-bias compensation [5].

The estimation problem is addressed for the CyberShip II vessel, whose model is nonlinear due to trigonometric kinematics, hydrodynamic terms, and the angular nature of the heading state. Under these conditions, sequential first-order linearization becomes less suitable, since the required Jacobians depend strongly on the operating point. A model-based Unscented Kalman Filter (UKF) is thus adopted. The UKF propagates a set of *sigma* points (deterministic, carefully chosen sample points that represent a probability distribution, typically Gaussian, in terms of its mean and covariance) through the nonlinear process and measurement models, avoiding explicit Jacobian computation and reducing the approximation errors that may affect Extended Kalman Filter (EKF)-based navigation in nonlinear systems [6], [7]. In addition, IMU biases are included as states because they are slowly varying error sources that can significantly reduce estimation accuracy if not compensated for [3]. Their inclusion allows aiding measurements to constrain position, heading, velocity, and inertial-error growth [8]. Accordingly, a multi-rate fusion architecture is adopted. In this structure, the IMU supports the high-rate prediction step, while GNSS and compass measurements provide lower-rate corrections to limit drift accumulation [3], [9]. Therefore, the model-based UKF fusion of GNSS, compass, and IMU measurements provides a suitable

This work was supported by Grant PID2024-158365OB-C22 (CONDOR), funded by MICIU/AEI/10.13039/501100011033. Luis Orihuela was supported by the Agencia Estatal de Investigación through the Ramón y Cajal fellowship under Grant RYC2021-032919-I. Corresponding author: Sajjad Fakhar Shahreza, sfakhar@uloyola.es.

framework for nonlinear state estimation with better continuity and robustness than GNSS-only positioning [7], [9], [10].

The remainder of this paper is organized as follows. Section II presents the CyberShip II model and the main sources of nonlinearity. Section III describes the sensor models and the augmented-state formulation. Section IV introduces the multi-rate UKF implementation. Section V reports the simulation study, including the configuration and filter comparison. Finally, Section VI presents the main conclusions and future work.

II. Vessel model and sources of nonlinearity

The 3-degree-of-freedom (DOF) motion of the CyberShip II vessel is described using the Earth-fixed North-East-Down (NED) {n} and the body-fixed {b} frames [11]. The pose and velocity vectors are defined as $\boldsymbol{\eta} = [x\ y\ \psi]^\top$ and $\boldsymbol{\nu} = [u\ v\ r]^\top$, where x, y are the planar coordinates, ψ is the heading, and u, v, and r are the surge, sway, and yaw velocities, respectively.

The 3-DOF vessel model is expressed in (1) [11]:

$$\begin{cases} \dot{\boldsymbol{\eta}} = \boldsymbol{\mathcal{R}}(\psi)\boldsymbol{\nu}, \\ \boldsymbol{\mathcal{M}}\dot{\boldsymbol{\nu}} = -\boldsymbol{\mathcal{C}}(\boldsymbol{\nu})\boldsymbol{\nu} - \boldsymbol{\mathcal{D}}(\boldsymbol{\nu})\boldsymbol{\nu} + \boldsymbol{\tau}_w + \boldsymbol{\tau}, \end{cases} \tag{1}$$

where $\boldsymbol{\mathcal{R}}(\psi)$ is the rotation matrix between {b} and {n}, while $\boldsymbol{\mathcal{M}}$, $\boldsymbol{\mathcal{C}}(\boldsymbol{\nu})$, and $\boldsymbol{\mathcal{D}}(\boldsymbol{\nu})$ are the inertia, Coriolis–centrifugal, and damping matrices, respectively. The vector $\boldsymbol{\tau} = [F_u \quad 0 \quad \tau_r]^\top$ represents the commanded generalised forces, while $\boldsymbol{\tau}_w$ represents external disturbances [11]. As reported in [12], CyberShip II is a fully actuated vessel. However, in this work, as in several studies in the literature, an underactuated input configuration is considered by neglecting the sway force.

In the estimator design, the vessel kinetics is expressed in terms of acceleration. The input gain $\boldsymbol{G}$ is defined as $\boldsymbol{G} = \boldsymbol{\mathcal{M}}^{-1}\boldsymbol{\tau} = [G_u\ G_v\ G_r]^\top$. Therefore, the velocity dynamics can be rewritten as in (2), where $\boldsymbol{\sigma}_h(\boldsymbol{\nu})$ represents the modeled hydrodynamics and $\boldsymbol{\sigma}_e$ contains residual lumped disturbances:

$$\dot{\boldsymbol{\nu}} = \boldsymbol{G} + \boldsymbol{\sigma}_h(\boldsymbol{\nu}) + \boldsymbol{\sigma}_e, \tag{2a}$$

$$\boldsymbol{\sigma}_h = [\sigma_{uh}\ \sigma_{vh}\ \sigma_{rh}]^\top = -\boldsymbol{\mathcal{M}}^{-1}(\boldsymbol{\mathcal{C}}(\boldsymbol{\nu})\boldsymbol{\nu} + \boldsymbol{\mathcal{D}}(\boldsymbol{\nu})\boldsymbol{\nu}), \tag{2b}$$

$$\boldsymbol{\sigma}_e = [\sigma_{ue}\ \sigma_{ve}\ \sigma_{re}]^\top = \boldsymbol{\mathcal{M}}^{-1}\boldsymbol{\tau}_w. \tag{2c}$$

Assumption II.1. The residual disturbances $\boldsymbol{\sigma}_e$ are assumed to vary slowly during the estimation process and modeled as a continuous-time random-walk state, following standard practice for slowly varying marine disturbances [13], [14]:

$$\dot{\boldsymbol{\sigma}}_e = \boldsymbol{w}_\sigma(t), \tag{3}$$

where $\boldsymbol{w}_\sigma(t)$ is zero-mean Gaussian white process noise. Therefore, in the nominal model, $\mathbb{E}[\dot{\boldsymbol{\sigma}}_e] = \mathbf{0}$. The disturbance-related process-noise covariance is denoted by:

$$\boldsymbol{Q}_\sigma = \mathrm{Cov}(\boldsymbol{w}_\sigma(t)). \tag{4}$$

This matrix $\boldsymbol{Q}_\sigma$ represents only the sub-block of the process-noise covariance associated with the random-walk dynamics of $\boldsymbol{\sigma}_e$. The complete process-noise covariance matrix $\boldsymbol{Q}$, which covers all augmented states, will be defined in Section IV.

The damping matrix $\boldsymbol{\mathcal{D}}(\boldsymbol{\nu})$ follows the identified ship model reported in [12]. Since both $\boldsymbol{\mathcal{C}}$ and $\boldsymbol{\mathcal{D}}$ depend on the body-fixed velocities $\boldsymbol{\nu}$, the process model remains explicitly nonlinear.

III. Sensors and measurement models

The sensor configuration considered in this work is summarized in Table I. The listed sampling rates correspond to the simulation setup used in this work. The control input $\boldsymbol{\tau}$ is assumed known and is thus not included in the output vector.

TABLE I: Measurements and sampling rates used in simulation

Sensor	Measured variable	Unit	Frequency
GNSS	(x, y)	m	10 Hz
AHRS / compass	ψ	rad	10 Hz
IMU accelerometers	(a_u, a_v)	$\mathrm{m\,s^{-2}}$	100 Hz
Gyroscope	r	$\mathrm{rad\,s^{-1}}$	100 Hz

The complete output vector is defined as in (5):

$$\boldsymbol{z}_{\text{full}} = \begin{bmatrix} x_m & y_m & \psi_m & a_{u_m} & a_{v_m} & r_m \end{bmatrix}^\top \in \mathbb{R}^6. \tag{5}$$

Variables with subscript m denote measured values, while variables without this subscript denote the corresponding true variables. The measurement-noise terms are denoted by n_i, with $i \in \{x, y, \psi, au, av, \omega\}$ and are assumed to be zero-mean Gaussian, mutually independent, uncorrelated with time, and with variance q_i, i.e. $n_i \sim \mathcal{N}(0, q_i)$.

The GNSS position and heading measurements are assumed to be unbiased and only affected by additive noise as in (6):

$$x_m = x + n_x, \qquad y_m = y + n_y, \qquad \psi_m = \psi + n_\psi. \tag{6}$$

The gyroscope measurement is assumed to be affected by additive noise and a slowly varying bias b_ω:

$$r_m = r + b_\omega + n_\omega, \tag{7}$$

The accelerometer channels are also affected by additive noise and slowly varying biases. In the body-fixed frame, they are modeled as in (8):

$$a_{u_m} = \dot{u} + g_x + b_{au} + n_{au}, \quad a_{v_m} = \dot{v} + g_y + b_{av} + n_{av}, \tag{8}$$

where b_{au} and b_{av} are the accelerometer biases. The time-varying gravity contributions are given by $g_x = g\sin(\theta)$ and $g_y = -g\sin(\phi)\cos(\theta)$, where g is the gravitational acceleration and ϕ and θ denote the roll and pitch angles, respectively, provided by the IMU at each sampling instant. This separation between slowly varying bias and zero-mean random noise follows standard GNSS/IMU modelling assumptions in navigation and state estimation [3], [11].

Assumption III.1. The vessel dynamics is modeled in planar 3-DOF, but attitude information from the IMU is also available.

For the inertial sensors, the measurement errors are composed of bias and random noise. Therefore, at each time instant:

$$e_\omega = b_\omega + n_\omega, \quad e_{au} = b_{au} + n_{au}, \quad e_{av} = b_{av} + n_{av}, \tag{9}$$

with $e_j \sim \mathcal{N}(b_j, q_i),\ j \in \{\omega, au, av\}$, where e_ω is the total gyroscope error, and e_{au} and e_{av} are part of the accelerometer

errors in the surge and sway directions. The variances q_i with $i \in \{x, y, \psi, au, av, \omega\}$ are assumed to be known for the estimator design. The bias signals are known in simulation only for generating synthetic measurements and evaluating the estimation error. During filtering, they are treated as unknown slowly varying states, as in a real experimental case. The measurement-noise covariance matrix contains only the variances of the zero-mean random noise components, i.e. $\boldsymbol{R} = \mathrm{diag}\,(q_x, q_y, q_\psi, q_{au}, q_{av}, q_\omega)$.

Problem formulation and augmented states

In the considered sensor configuration, the complete velocity vector $\boldsymbol{\nu}$ is not available as a direct noiseless measurement. Thus, velocities must be reconstructed from the nonlinear process model and the available sensors. The measurement-noise vector satisfies the stochastic model defined in Section III.

Assumption III.2. The gyroscope bias b_ω and the accelerometer bias vector $\boldsymbol{b}_a = [b_{au}\ b_{av}]^\top$ are modeled as slowly varying random-walk states.

Let $\boldsymbol{x}_k$ denote the augmented state vector of the estimator at discrete time k, and let $\hat{\boldsymbol{x}}_k$ denote its estimate. The estimation error is defined as $\boldsymbol{e}_k = \boldsymbol{x}_k - \hat{\boldsymbol{x}}_k$. The objective is to design a state estimator that minimizes, at each time instant, the variance of the estimation error, i.e. $\mathbb{E}\left[\|\boldsymbol{e}_k\|^2\right]$. This objective must be achieved under model nonlinearities, sensor noise, multi-rate measurements Table I, inertial biases, and residual disturbances.

Consider a planar vessel whose dynamics is given by (2) under the disturbance modelling assumption of Section II. The measurements in (5) satisfy the stochastic noise model presented in Section III, with covariance matrix $\boldsymbol{R}$.

(a) For the complete measurement vector $\boldsymbol{z}_{\mathrm{full},k}$ in (5), the objective is to estimate the augmented state vector $\boldsymbol{x}_{IA,k}$:

$$\boldsymbol{x}_{IA,k} = [\boldsymbol{\eta}^\top\ \boldsymbol{\nu}^\top\ \boldsymbol{b}_a^\top\ b_\omega\ \boldsymbol{\sigma}_e^\top]^\top \in \mathbb{R}^{12}, \tag{10}$$

while minimizing the variance of the estimation error $\boldsymbol{e}_{IA,k} = \boldsymbol{x}_{IA,k} - \hat{\boldsymbol{x}}_{IA,k}$. This formulation uses high-rate acceleration measurements to improve the estimation of fast transients.

(b) Consider the reduced measurement vector $\boldsymbol{z}_{GN,k}$ in (11):

$$\boldsymbol{z}_{GN,k} = [x_m\ y_m\ \psi_m\ r_m]^\top, \tag{11}$$

where the accelerometer biases cannot be observed because position, heading, and yaw measurements do not provide direct information about them. Therefore, including $\boldsymbol{b}_a$ would increase the state dimension without improving the estimate and could affect filter consistency through unnecessary cross-covariances [8]. The objective is to estimate the augmented state vector $\boldsymbol{x}_{GN,k}$ as in (12) while minimizing the variance of the estimation error $\boldsymbol{e}_{GN,k} = \boldsymbol{x}_{GN,k} - \hat{\boldsymbol{x}}_{GN,k}$:

$$\boldsymbol{x}_{GN,k} = [\boldsymbol{\eta}^\top\ \boldsymbol{\nu}^\top\ b_\omega\ \boldsymbol{\sigma}_e^\top]^\top \in \mathbb{R}^{10}. \tag{12}$$

IV. Unscented Kalman filter formulation

The UKF is formulated for the nonlinear discrete-time system

$$\boldsymbol{x}_{k+1} = f(\boldsymbol{x}_k, \boldsymbol{\tau}_k, \boldsymbol{w}_k), \qquad \boldsymbol{z}_k = h(\boldsymbol{x}_k, \boldsymbol{\tau}_k) + \boldsymbol{v}_k, \tag{13}$$

where $\boldsymbol{x}_k$, $\boldsymbol{\tau}_k$, and $\boldsymbol{z}_k$ are the state, input, and measurement vectors, and $\boldsymbol{w}_k$ and $\boldsymbol{v}_k$ are the process and measurement noise terms with covariances $\boldsymbol{Q}$ and $\boldsymbol{R}$, respectively. The process-noise covariance matrix $\boldsymbol{Q}$ is block-diagonal and covers all augmented states, with the disturbance block corresponding to the discretized version of $\boldsymbol{Q}_\sigma$ defined in (4). The nonlinear state-transition function $f(\cdot)$ is consistent with the vessel dynamics (1)–(2a), including the hydrodynamic and disturbance terms in (2b)–(2c). At each update, the measurement function $h(\cdot)$ uses the model for the available sensors, either the full vector in (5) or the reduced vector in (11).

With additive process noise, the state propagation implemented in the UKF can therefore be written equivalently as $\boldsymbol{x}_{k+1} = F_d(\boldsymbol{x}_k, \boldsymbol{\tau}_k) + \boldsymbol{w}_k$, where $\boldsymbol{w}_k \sim \mathcal{N}(\boldsymbol{0}, \boldsymbol{Q})$. The discrete transition function $F_d(\cdot)$ is obtained from the continuous-time nonlinear process model $f_c(\cdot)$ using forward Euler discretization, i.e., $F_d(\boldsymbol{x}_k, \boldsymbol{\tau}_k) = \boldsymbol{x}_k + \Delta t \cdot f_c(\boldsymbol{x}_k, \boldsymbol{\tau}_k)$, thus implementing $f_c(\cdot)$ in discrete time.

The logic of the multi-rate UKF implementation is organized in three steps.

Sampling. At each IMU step, the input $\boldsymbol{u}_{k-1}$ is read. Since $\Delta t_{\mathrm{IMU}} = 0.01$ s and $\Delta t_{\mathrm{GNSS}} = 0.1$ s, one GNSS/navigation sample is available every $N_r = 10$ IMU samples. Thus, the full correction is applied when $\mathrm{mod}(k, N_r) = 0$.

Prediction. The *sigma* points $\mathcal{X}_{k-1}^{(i)}$ are generated and propagated through $F_d(\cdot)$ to obtain $\hat{\mathcal{X}}_k^{(i)}$. The predicted state $\hat{\boldsymbol{x}}_k^-$ and covariance $\boldsymbol{P}_k^-$ are then computed.

Correction. Filter-IA uses $\boldsymbol{z}_{\mathrm{full},k}$ when GNSS/navigation data are available, and $\boldsymbol{z}_{IA,\mathrm{imu},k}$, defined in (14), otherwise. Filter-GN is corrected only with $\boldsymbol{z}_{GN,k}$. These steps are detailed in Algorithm 1.

$$\boldsymbol{z}_{IA,\mathrm{imu}} = \begin{bmatrix} a_{u_m} & a_{v_m} & r_m \end{bmatrix}^\top \in \mathbb{R}^{3\times 1}. \tag{14}$$

For a p-dimensional state vector $\boldsymbol{x}_k$, the scaled UKF uses $2p+1$ *sigma* points. Scaling parameters λ and γ are defined in (15), where α and κ control the spread of the *sigma* points around the mean value:

$$\lambda = \alpha^2(p+\kappa) - p, \qquad \gamma = \sqrt{p+\lambda}, \tag{15}$$

Let $\hat{\boldsymbol{x}}_{k-1|k-1}$ and $\boldsymbol{P}_{k-1|k-1}$ denote the posterior (filtered) state estimate and covariance at time $k-1$. For notational simplicity we write $\hat{\boldsymbol{x}}_{k-1} = \hat{\boldsymbol{x}}_{k-1|k-1}$ and $\boldsymbol{P}_{k-1} = \boldsymbol{P}_{k-1|k-1}$. The *sigma* points are generated as in (16)–(18):

$$\mathcal{X}_{k-1}^{(0)} = \hat{\boldsymbol{x}}_{k-1}, \tag{16}$$

$$\mathcal{X}_{k-1}^{(i)} = \hat{\boldsymbol{x}}_{k-1} + \gamma \left[\sqrt{\boldsymbol{P}_{k-1}}\right]_i, \qquad i = 1, \ldots, p, \tag{17}$$

$$\mathcal{X}_{k-1}^{(i+n)} = \hat{\boldsymbol{x}}_{k-1} - \gamma \left[\sqrt{\boldsymbol{P}_{k-1}}\right]_i, \qquad i = 1, \ldots, p, \tag{18}$$

where $\left[\sqrt{\boldsymbol{P}_{k-1}}\right]_i$ denotes the i-th column of a matrix square root of $\boldsymbol{P}_{k-1}$, obtained by Cholesky decomposition.

The weights of the mean and covariance are defined in (19):

$$W_0^m = \frac{\lambda}{p+\lambda}, \qquad W_0^c = \frac{\lambda}{p+\lambda} + (1 - \alpha^2 + \beta), \tag{19a}$$

$$W_i^m = W_i^c = \frac{1}{2(p+\lambda)}, \qquad i = 1, \ldots, 2p, \tag{19b}$$

Algorithm 1 Multi-rate implementation of the proposed filters

Require: $\hat{\boldsymbol{x}}_{IA,0}$, $\hat{\boldsymbol{x}}_{GN,0}$, $\boldsymbol{P}_{IA,0}$, $\boldsymbol{P}_{GN,0}$
Require: Total number of IMU samples N_{IMU}
Require: $\Delta t_{\mathrm{IMU}} = 0.01$ s, $\Delta t_{\mathrm{GNSS}} = 0.1$ s, $N_r = \Delta t_{\mathrm{GNSS}}/\Delta t_{\mathrm{IMU}} = 10$
for $k = 1, \ldots, N_{\mathrm{IMU}}$ **do**
  $t_{k-1} \leftarrow (k-1)\Delta t_{\mathrm{IMU}}$
  $\boldsymbol{\tau}_{k-1} \leftarrow \boldsymbol{\tau}(t_{k-1})$

A. Filter-IA update
  Prediction at IMU rate
  Generate $\mathcal{X}^{(i)}_{IA,k-1}$ from $\hat{\boldsymbol{x}}_{IA,k-1}$ and $\boldsymbol{P}_{IA,k-1}$
  $\hat{\mathcal{X}}^{(i)}_{IA,k} \leftarrow F_d(\mathcal{X}^{(i)}_{IA,k-1}, \boldsymbol{\tau}_{k-1})$
  Compute $\hat{\boldsymbol{x}}^{-}_{IA,k}$ and $\boldsymbol{P}^{-}_{IA,k}$ from $\hat{\mathcal{X}}^{(i)}_{IA,k}$
  if $\mathrm{mod}(k, N_r) = 0$ **then**
    Full correction
    $\boldsymbol{z}_{\mathrm{full},k} \leftarrow [x_m \; y_m \; \psi_m \; a_{um} \; a_{vm} \; r_m]^\top$
    $\mathcal{Z}^{(i)}_{IA,k} \leftarrow h_{IA}(\hat{\mathcal{X}}^{(i)}_{IA,k})$
    Compute $\hat{\boldsymbol{z}}_{IA,k}$ from $\mathcal{Z}^{(i)}_{IA,k}$
    Correct $\hat{\boldsymbol{x}}^{-}_{IA,k}$ and $\boldsymbol{P}^{-}_{IA,k}$ using $\boldsymbol{z}_{\mathrm{full},k}$ and $\hat{\boldsymbol{z}}_{IA,k}$
  else
    Inertial correction
    $\boldsymbol{z}_{IA,\mathrm{imu},k} \leftarrow [a_{um} \; a_{vm} \; r_m]^\top$
    $\mathcal{Z}^{(i)}_{IA,\mathrm{imu},k} \leftarrow h_{IA,\mathrm{imu}}(\hat{\mathcal{X}}^{(i)}_{IA,k})$
    Compute $\hat{\boldsymbol{z}}_{IA,\mathrm{imu},k}$ from $\mathcal{Z}^{(i)}_{IA,\mathrm{imu},k}$
    Correct $\hat{\boldsymbol{x}}^{-}_{IA,k}$ and $\boldsymbol{P}^{-}_{IA,k}$ using $\boldsymbol{z}_{IA,\mathrm{imu},k}$ and $\hat{\boldsymbol{z}}_{IA,\mathrm{imu},k}$
  end if

B. Filter-GN update
  if $\mathrm{mod}(k, N_r) = 0$ **then**
    Prediction at GNSS/navigation rate
    Generate $\mathcal{X}^{(i)}_{GN,k-1}$ from $\hat{\boldsymbol{x}}_{GN,k-1}$ and $\boldsymbol{P}_{GN,k-1}$
    $\hat{\mathcal{X}}^{(i)}_{GN,k} \leftarrow F_d(\mathcal{X}^{(i)}_{GN,k-1}, \boldsymbol{\tau}_{k-1})$
    Compute $\hat{\boldsymbol{x}}^{-}_{GN,k}$ and $\boldsymbol{P}^{-}_{GN,k}$ from $\hat{\mathcal{X}}^{(i)}_{GN,k}$
    Correction
    $\boldsymbol{z}_{GN,k} \leftarrow [x_m \; y_m \; \psi_m \; r_m]^\top$
    $\mathcal{Z}^{(i)}_{GN,k} \leftarrow h_{GN}(\hat{\mathcal{X}}^{(i)}_{GN,k})$
    Compute $\hat{\boldsymbol{z}}_{GN,k}$ from $\mathcal{Z}^{(i)}_{GN,k}$
    Correct $\hat{\boldsymbol{x}}^{-}_{GN,k}$ and $\boldsymbol{P}^{-}_{GN,k}$ using $\boldsymbol{z}_{GN,k}$ and $\hat{\boldsymbol{z}}_{GN,k}$
  else
    $\hat{\boldsymbol{x}}_{GN,k} \leftarrow \hat{\boldsymbol{x}}_{GN,k-1}$
    $\boldsymbol{P}_{GN,k} \leftarrow \boldsymbol{P}_{GN,k-1}$
  end if

  $\hat{\psi}_{IA,k} \leftarrow \mathrm{wrap}(\hat{\psi}_{IA,k})$
  $\hat{\psi}_{GN,k} \leftarrow \mathrm{wrap}(\hat{\psi}_{GN,k})$
end for

where the control parameter β includes prior information about the state distribution. Each *sigma* point is then propagated through the discrete-time nonlinear process model, as in (20):

$$\hat{\mathcal{X}}^{(i)}_k = F_d\Big(\mathcal{X}^{(i)}_{k-1}, \boldsymbol{u}_{k-1}\Big), \qquad i = 0, \ldots, 2p. \tag{20}$$

The predicted state mean and covariance are computed from the propagated *sigma* points as indicated in (21)–(22):

$$\hat{\boldsymbol{x}}^{-}_k = \sum_{i=0}^{2p} W^m_i \hat{\mathcal{X}}^{(i)}_k, \tag{21}$$

$$\boldsymbol{P}^{-}_k = \sum_{i=0}^{2p} W^c_i \left(\hat{\mathcal{X}}^{(i)}_k - \hat{\boldsymbol{x}}^{-}_k\right)\left(\hat{\mathcal{X}}^{(i)}_k - \hat{\boldsymbol{x}}^{-}_k\right)^\top + \boldsymbol{Q}. \tag{22}$$

For the measurement update, the propagated *sigma* points are mapped through the active measurement model as in (23):

$$\mathcal{Z}^{(i)}_k = h\Big(\hat{\mathcal{X}}^{(i)}_k\Big), \qquad i = 0, \ldots, 2p. \tag{23}$$

The predicted measurement mean is then computed as in (24):

$$\hat{\boldsymbol{z}}_k = \sum_{i=0}^{2p} W^m_i \mathcal{Z}^{(i)}_k. \tag{24}$$

The innovation covariance and the state-measurement cross-covariance are given by (25)–(26):

$$\boldsymbol{S}_k = \sum_{i=0}^{2p} W^c_i \left(\mathcal{Z}^{(i)}_k - \hat{\boldsymbol{z}}_k\right)\left(\mathcal{Z}^{(i)}_k - \hat{\boldsymbol{z}}_k\right)^\top + \boldsymbol{R}, \tag{25}$$

$$\boldsymbol{P}_{xz,k} = \sum_{i=0}^{2p} W^c_i \left(\hat{\mathcal{X}}^{(i)}_k - \hat{\boldsymbol{x}}^{-}_k\right)\left(\mathcal{Z}^{(i)}_k - \hat{\boldsymbol{z}}_k\right)^\top. \tag{26}$$

The Kalman gain and the posterior state update are then computed as in (27)–(29):

$$\boldsymbol{K}_k = \boldsymbol{P}_{xz,k}\boldsymbol{S}^{-1}_k, \tag{27}$$

$$\hat{\boldsymbol{x}}_k = \hat{\boldsymbol{x}}^{-}_k + \boldsymbol{K}_k\left(\boldsymbol{z}_k - \hat{\boldsymbol{z}}_k\right), \tag{28}$$

$$\boldsymbol{P}_k = \boldsymbol{P}^{-}_k - \boldsymbol{K}_k\boldsymbol{S}_k\boldsymbol{K}^\top_k. \tag{29}$$

Thus, $\hat{\boldsymbol{x}}^{-}_k$ and $\boldsymbol{P}^{-}_k$ correspond to the prior estimates $\hat{\boldsymbol{x}}_{k|k-1}$ and $\boldsymbol{P}_{k|k-1}$, whereas $\hat{\boldsymbol{x}}_k$ and $\boldsymbol{P}_k$ correspond to the posterior (filtered) estimates $\hat{\boldsymbol{x}}_{k|k}$ and $\boldsymbol{P}_{k|k}$.

For Filter-IA, the measurement function $h_{IA}(\boldsymbol{x}_{IA})$ is:

$$h_{IA}(\boldsymbol{x}_{IA}) = \begin{bmatrix} x \\ y \\ \psi \\ G_u + \sigma_{uh} + \sigma_{ue} + g_x + b_{au} \\ G_v + \sigma_{vh} + \sigma_{ve} + g_y + b_{av} \\ r + b_\omega \end{bmatrix}. \tag{30}$$

For Filter-GN, the reduced measurement vector in (11) is used and the measurement function $h_{GN}(\boldsymbol{x}_{GN})$ is:

$$h_{GN}(\boldsymbol{x}_{GN}) = [x \quad y \quad \psi \quad r + b_\omega]^\top. \tag{31}$$

These measurement functions map the augmented states to the measurement vectors defined in Section III. The function h_{IA} yields the full measurement vector in (5), and h_{GN} yields the reduced measurement vector in (11). The UKF selects the measurement vector and model based on the available sensors, as shown in Algorithm 1. During low-rate updates, Filter-IA uses the full measurement vector (5) along with the measurement function (30). During high-rate updates between two low-rate measurements, only the inertial subset given by (32), compliant with (14), is used:

$$h_{IA,\mathrm{imu}}(\boldsymbol{x}_{IA}) = \begin{bmatrix} G_u + \sigma_{uh} + \sigma_{ue} + g_x + b_{au} \\ G_v + \sigma_{vh} + \sigma_{ve} + g_y + b_{av} \\ r + b_\omega \end{bmatrix}. \tag{32}$$

Since the heading is an angular state, it is wrapped to $(-\pi, \pi]$ after propagation and also when the innovation is computed. The multi-rate implementation is handled by selecting, at each update instant, the measurement vector, measurement function, and covariance matrix related to the sensors available at that time. Therefore, Filter-IA, with $p = 12$, uses 25 sigma points, while Filter-GN, with $p = 10$, uses 21 sigma points.

V. Simulation Study

A. Simulation configuration

The simulations are performed in MATLAB using the CyberShip II model from the Marine Systems Simulator (MSS) library [15]. Zero-mean sensor noise is added according to the measurement models in Section III. Three cases are analyzed: two straight-line surge excitations and one circular-motion case. In the straight-line cases, $\tau_r = 0$ and the sawtooth surge-force profiles shown in Fig. 1, with $2\,\mathrm{s}$ and $10\,\mathrm{s}$ ramps, are applied. The circular case is generated with constant F_u and τ_r.

Both filters use the same measurement-noise covariance. The main tuning difference is introduced through the process-noise covariance. Since Filter-IA uses high-rate accelerometer measurements, while Filter-GN relies on position, heading, and gyroscope yaw measurements, Filter-GN's velocity-related process noise is tuned more conservatively to reduce model dependence during rapid input variations.

The covariance matrices are block diagonal. For both filters, the initial variances of x, y, ψ, u, v, and r are set to 0.1, 0.1, $(\pi/180)^2$, 0.01, 0.04, and 0.01, respectively. The gyroscope-bias variance is 0.1, the accelerometer-bias variances in Filter-IA are 0.3, and the residual disturbance variances are 0.1 for σ_{ue} and 0.001 for σ_{ve} and σ_{re}. The process-noise standard deviations are set to $\sigma_x = \sigma_y = \sigma_\psi = \sigma_{b_\omega} = \sigma_{bau} = \sigma_{bav} = \sigma_{eu} = \sigma_{ev} = \sigma_{er} = 10^{-3}$, with $\sigma_u = \sigma_v = 5 \cdot 10^{-3}$ and $\sigma_r = 2 \cdot 10^{-3}$. The UKF parameters are set to $\beta = 2$, according to [6], $\alpha = 10^{-3}$, and $\kappa = -0.1$.

B. Results and filter comparison

This section compares Filter-IA and Filter-GN for the aforementioned cases. The straight-line cases evaluate the effect of surge-excitation rate on the velocity estimates, while the circular case assesses coupled translational/rotational dynamics. The $2\,\mathrm{s}$ ramp case is more demanding and shows more clearly how the tuning of the process-noise covariance affects the filter behavior. Fig. 2 compares the surge estimates of two filters with the true value for the $2\,\mathrm{s}$ ramp case. The inset highlights the local tracking behavior and the smoothness of the estimates. With the same process-noise covariance, Filter-GN shows a clear bias in tracking the true surge. In contrast, Filter-IA remains closer to the true response because the high-rate accelerometer measurements provide additional correction information. This difference is especially visible in the inset.

Fig. 3 shows that increasing the velocity-related process-noise entries of Filter-GN reduces the bias observed in Fig. 2. The latter follows the true surge more closely, though its estimate remains less smooth than that of Filter-IA. This indicates that, under fast excitation, the main limitation of Filter-GN is its greater dependence on the process model, rather than filter instability. For the $10\,\mathrm{s}$ ramp case, the surge excitation is smoother, and the vessel dynamics change more gradually. As shown in Fig. 4, Filter-GN tracks the true surge with acceptable accuracy. Thus, the reduced filter remains a valid option for slower transients, where the model and lower-rate aiding measurements are enough to reconstruct the motion.

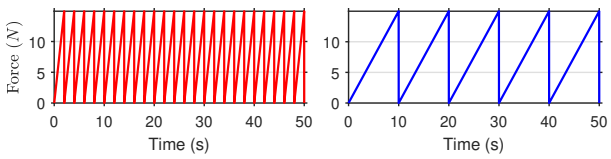


Fig. 1: Sawtooth surge-force profiles with $2\,\mathrm{s}$ and $10\,\mathrm{s}$ ramps.

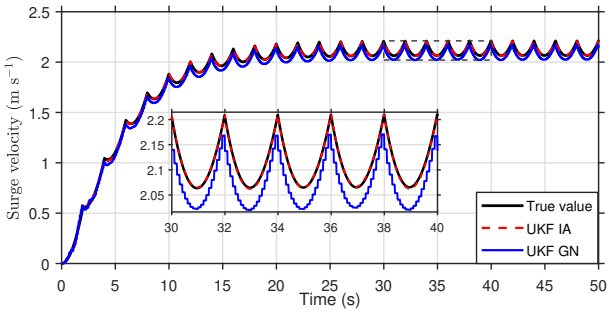


Fig. 2: $2\,\mathrm{s}$ ramp: surge velocity estimation comparison.

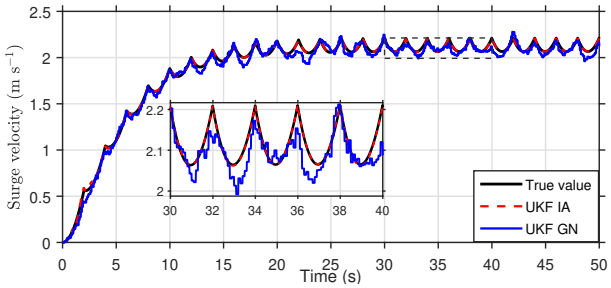


Fig. 3: $2\,\mathrm{s}$ ramp: tuned Filter-GN covariance.

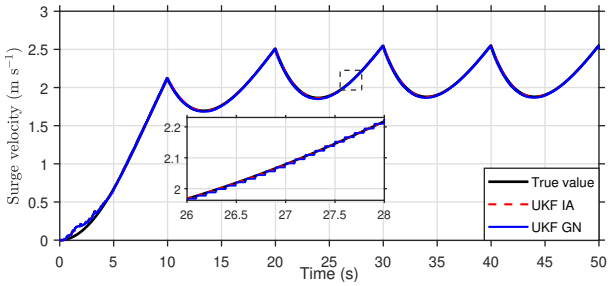


Fig. 4: $10\,\mathrm{s}$ ramp: surge velocity estimation comparison.

The circular-motion case is finally considered to evaluate the filters under coupled translational and rotational dynamics. Unlike the straight-line cases, where the primary differences appear mainly in the surge estimates, this test allows analysis of trajectory reconstruction and rotational behavior. For this reason, the comparison is presented in terms of yaw estimation and the reconstructed horizontal-plane trajectory. Fig. 5 and 6 show that both filters reconstruct the circular motion with good accuracy despite noisy measurements. The yaw estimates remain consistent with the true rotational response, while the trajectory plot shows that both filters smooth the scattered

GNSS measurements. Filter-IA provides the smoothest estimate and stays slightly closer to the true path, whereas Filter-GN still reconstructs the coupled motion with acceptable accuracy.

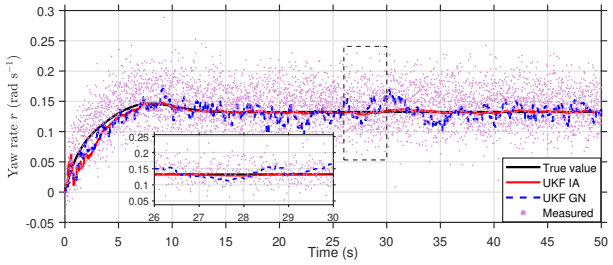


Fig. 5: Circular-motion case: yaw-rate estimation.

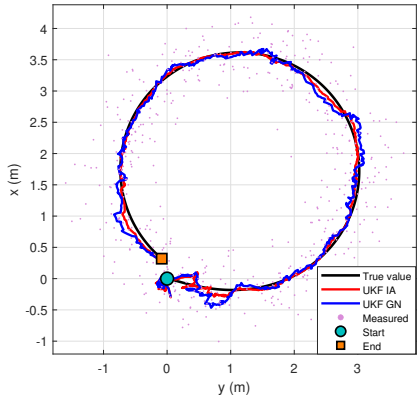


Fig. 6: Circular-motion trajectory.

Table II reports Root Mean Square Error (RMSE) values for the 10 s ramp and circular-motion cases. Filter-IA gives lower errors, while Filter-GN still provides acceptable reconstruction.

TABLE II: RMSEs of estimated states in 2 different scenarios

		10 s ramp		Circular trajectory	
Estimated state	Unit	Filter-IA	Filter-GN	Filter-IA	Filter-GN
x	m	0.078495	0.088235	0.075240	0.100452
y	m	0.073758	0.093094	0.061580	0.092373
ψ	rad	0.031618	0.045714	0.034166	0.050055
u	m/s	0.048115	0.039873	0.056276	0.063806
v	m/s	0.027905	0.04729	0.017674	0.028661
r	rad/s	0.025482	0.031346	0.019194	0.028414
b_{au}	m/s^2	0.034585	–	0.030682	–
b_{av}	m/s^2	0.022355	–	0.016937	–
b_{ω}	rad/s	0.025935	0.025971	0.019838	0.021719
σ_{ue}	m/s^2	0.016884	0.033441	0.020944	0.030470
σ_{ve}	m/s^2	0.0063366	0.0084162	0.005761	0.009731
σ_{re}	rad/s^2	0.013767	0.090652	0.012227	0.052826

VI. Conclusions

This paper presents and compares two UKF estimators — Filter-IA and Filter-GN — for state estimation of the CyberShip II vessel. The simulation results show that Filter-IA provides smoother, more accurate estimates, especially for velocity-related states, by using high-rate accelerometer measurements in the correction step. This improves short-term dynamic reconstruction and reduces lag under fast input variations. Therefore, Filter-IA is preferable under GNSS-degraded conditions, such as bridges or urban canyons, where IMU measurements can support estimation continuity during temporary GNSS outages. In contrast, Filter-GN has a simpler structure, with a lower state dimension and fewer sensor requirements. It is suitable when only GNSS position, compass heading, and gyroscope yaw measurements are available, or when accelerometer channels are excluded. Although its accuracy decreases under fast excitation because it depends more on the process model, it still provides acceptable estimates under slower or moderately dynamic conditions. Moreover, the results show that proper tuning of the process-noise covariance can mitigate its limitations. This behavior is consistent with the observability properties of each filter. The accelerometer biases are locally observable in Filter-IA, whereas their exclusion from Filter-GN is justified by the reduced measurement set.

Future work will focus on extending the proposed framework beyond simulation. Indeed, experimental verification is required to assess robustness under realistic environmental disturbances, sensor imperfections, and GNSS degradation.

References

[1] E. Zereik, M. Bibuli, N. Mišković, P. Ridao, and A. Pascoal, "Challenges and future trends in marine robotics," *Annu. Rev. Control*, vol. 46, pp. 350–368, 2018.

[2] S. Y. Alaba, "GPS-IMU sensor fusion for reliable autonomous vehicle position estimation," 2024. [Online]. Available: https://arxiv.org/abs/2405.08119

[3] T. Suzuki, "Attitude-estimation-free GNSS and IMU integration," *IEEE Robot. Autom. Lett.*, vol. 9, no. 2, pp. 1090–1097, 2024.

[4] R. Erfianti, T. Asfihani, and H. F. Suhandri, "GNSS/IMU sensor fusion performance comparison of a car localization in urban environment using extended Kalman filter," *IOP Conf. Ser.: Earth Environ. Sci.*, vol. 1127, no. 1, p. 012006, 2023.

[5] H. F. Grip, T. I. Fossen, T. A. Johansen, and A. Saberi, "Globally exponentially stable attitude and gyro bias estimation with application to GNSS/INS integration," *Autom.*, vol. 51, pp. 158–166, 2014.

[6] R. Van der Merwe, "Sigma-point Kalman filters for probabilistic inference in dynamic state-space models," Ph.D. dissertation, Oregon Health and Science University, 2004.

[7] C. Yang, W. Shi, and W. Chen, "Comparison of unscented and extended Kalman filters with application in vehicle navigation," *J. Navig.*, vol. 70, no. 2, pp. 411–431, 2016.

[8] S. Du, W. Sun, and Y. Gao, "Improving observability of an inertial system by rotary motions of an IMU," *Sens.*, vol. 17, no. 4, p. 698, 2017.

[9] M. Rhudy, Y. Gu, J. Gross, S. Gururajan, and M. R. Napolitano, "Sensitivity analysis of extended and unscented Kalman filters for attitude estimation," *J. Aerosp. Inf. Syst.*, vol. 10, no. 3, pp. 131–143, 2013.

[10] M. N. Cahyadi, T. Asfihani, H. F. Suhandri, and R. Erfianti, "Unscented Kalman filter for a low-cost GNSS/IMU-based mobile mapping application under demanding conditions," *Geod. Geodyn.*, vol. 15, no. 2, pp. 166–176, 2023.

[11] T. I. Fossen, *Handbook of Marine Craft Hydrodynamics and Motion Control*. Wiley, 2011.

[12] R. Skjetne, Ø. Smogeli, and T. I. Fossen, "Modeling, identification, and adaptive maneuvering of CyberShip II: A complete design with experiments," *IFAC Proc. Vol.*, vol. 37, no. 10, pp. 203–208, 2004.

[13] T. I. Fossen and J. P. Strand, "Passive nonlinear observer design for ships using Lyapunov methods: Full-scale experiments with a supply vessel," *Autom.*, vol. 35, pp. 3–16, 1999.

[14] T. I. Fossen and T. Perez, "Kalman filtering for positioning and heading control of ships and offshore rigs," *IEEE Control Systems Magazine*, vol. 29, pp. 32–46, 2009.

[15] T. I. Fossen and T. Perez, "Marine systems simulator (MSS)," https://github.com/cybergalactic/MSS, 2004.